

1 **Phylogenetic ctDNA analysis depicts early stage lung cancer evolution**

2

3 Christopher Abbosh<sup>1\*</sup>, Nicolai J. Birkbak<sup>1,2\*</sup>, Gareth A. Wilson<sup>1,2\*</sup>, Mariam Jamal-Hanjani<sup>1\*</sup>,  
4 Tudor Constantin<sup>3\*</sup>, Raheleh Salari<sup>3\*</sup>, John Le Quesne<sup>4\*</sup>, David A Moore<sup>4+</sup>, Selvaraju  
5 Veeriah<sup>1+</sup>, Rachel Rosenthal<sup>1+</sup>, Teresa Marafioti<sup>1,5</sup>, Eser Kirkizlar<sup>3</sup>, Thomas B K Watkins<sup>1,2</sup>,  
6 Nicholas McGranahan<sup>1,2</sup>, Sophia Ward<sup>1,2,6</sup>, Luke Martinson<sup>4</sup>, Joan Riley<sup>4</sup>, Francesco Fraioli<sup>7</sup>,  
7 Maise Al Bakir<sup>2</sup>, Eva Gronroos<sup>2</sup>, Francisco Zambrana<sup>1</sup>, Raymondo Endozo<sup>7</sup>, Wenya Linda  
8 Bi<sup>8,9</sup>, Fiona M. Fennessy<sup>8,9</sup>, Nicole Sponer<sup>3</sup>, Diana Johnson<sup>1</sup>, Joanne Laycock<sup>1</sup>, Seema Shafi<sup>1</sup>,  
9 Justyna Czyzewska-Khan<sup>1</sup>, Andrew Rowan<sup>2</sup>, Tim Chambers<sup>2,6</sup>, Nik Matthews<sup>6,10</sup>, Samra  
10 Turajlic<sup>2,11</sup>, Crispin Hiley<sup>1,2</sup>, Siow Ming Lee<sup>12,1</sup>, Martin Forster<sup>1,12</sup>, Tanya Ahmad<sup>12</sup>, Mary  
11 Falzon<sup>5</sup>, Elaine Borg<sup>5</sup>, David Lawrence<sup>13</sup>, Martin Hayward<sup>13</sup>, Shyam Kolvekar<sup>13</sup>, Nikolaos  
12 Panagiotopoulos<sup>13</sup>, Sam M Janes<sup>1,14,15</sup>, Ricky Thakrar<sup>14</sup>, Asia Ahmed<sup>16</sup>, Fiona Blackhall<sup>17,18</sup>,  
13 Yvonne Summers<sup>18</sup>, Dina Hafez<sup>3</sup>, Ashwini Naik<sup>3</sup>, Apratim Ganguly<sup>3</sup>, Stephanie Kareht<sup>3</sup>,  
14 Rajesh Shah<sup>19</sup>, Leena Joseph<sup>20</sup>, Anne Marie Quinn<sup>20</sup>, Phil Crosbie<sup>21</sup>, Babu Naidu<sup>22</sup>, Gary  
15 Middleton<sup>23</sup>, Gerald Langman<sup>24</sup>, Simon Trotter<sup>24</sup>, Marianne Nicolson<sup>25</sup>, Hardy Remmen<sup>26</sup>,  
16 Keith Kerr<sup>27</sup>, Mahendran Chetty<sup>28</sup>, Lesley Gomersall<sup>29</sup>, Dean Fennell<sup>4</sup>, Apostolos Nakas<sup>30</sup>,  
17 Sridhar Rathinam<sup>30</sup>, Girija Anand<sup>31</sup>, Sajid Khan<sup>32,33</sup>, Peter Russell<sup>34</sup>, Veni Ezhil<sup>35</sup>, Babikir  
18 Ismail<sup>36</sup>, Melanie Irvin-sellers<sup>37</sup>, Vineet Prakash<sup>38</sup>, Jason Lester<sup>39</sup>, Malgorzata  
19 Kornaszewska<sup>40</sup>, Richard Attanoos<sup>41</sup>, Haydn Adams<sup>42</sup>, Helen Davies<sup>43</sup>, Dahmane Oukrif<sup>1</sup>,  
20 Ayse U Akarca<sup>1</sup>, John A Hartley<sup>44</sup>, Helen L Lowe<sup>44</sup>, Sara Lock<sup>45</sup>, Natasha Iles<sup>46</sup>, Harriet Bell<sup>46</sup>,  
21 Yenting Ngai<sup>46</sup>, Greg Elgar<sup>2,6</sup>, Zoltan Szallasi<sup>47,48,49</sup>, Roland F Schwarz<sup>50</sup>, Javier Herrero<sup>51</sup>,  
22 Aengus Stewart<sup>52</sup>, Sergio A Quezada<sup>53</sup>, Peter Van Loo<sup>54,55</sup>, Caroline Dive<sup>56</sup>, Jimmy Lin<sup>3</sup>,  
23 Matthew Rabinowitz<sup>3</sup>, Hugo JWL Aerts<sup>8,9,57</sup>, Allan Hackshaw<sup>45</sup>, Jacqui A Shaw<sup>4</sup>, Bernhard G.  
24 Zimmermann<sup>3</sup>, and Charles Swanton<sup>1,2</sup> on behalf of the TRACERx and PEACE consortia.

25 \*These authors contributed equally to this work +These authors contributed equally to this work

- 26 1. Cancer Research UK Lung Cancer Centre of Excellence, University College London  
27 Cancer Institute, Paul O'Gorman Building, 72 Huntley Street, London, WC1E 6BT
- 28 2. Translational Cancer Therapeutics Laboratory, The Francis Crick Institute, 1 Midland  
29 Rd, London NW1 1AT
- 30 3. Natera Inc., 201 Industrial Rd., San Carlos, United States, CA 94070
- 31 4. Cancer Studies, University of Leicester, Leicester, United Kingdom, LE2 7LX
- 32 5. Department of Pathology, University College London Hospitals, 235 Euston Rd,  
33 Fitzrovia, London, United Kingdom, NW1 2BU
- 34 6. Advanced Sequencing Facility, The Francis Crick Institute, 1 Midland Rd, London  
35 NW1 1AT
- 36 7. Department of Nuclear Medicine, University College London Hospitals, 235 Euston  
37 Rd, Fitzrovia, London, United Kingdom, NW1 2BU
- 38 8. Brigham and Women's Hospital, Boston, MA 02115, USA
- 39 9. Harvard Medical School, Boston, MA 02115, USA
- 40 10. Tumour Profiling Unit Genomics Facility, The Institute of Cancer Research, 237  
41 Fulham Road, London, SW3 6JB
- 42 11. Renal and Skin Units, The Royal Marsden Hospital, London, SW3 6JJ
- 43 12. Department of Oncology, University College London Hospitals, 235 Euston Rd,  
44 Fitzrovia, London, United Kingdom, NW1 2BU
- 45 13. Department of Cardiothoracic Surgery, University College London Hospitals, 235  
46 Euston Rd, Fitzrovia, London, United Kingdom, NW1 2BU
- 47 14. Department of Respiratory Medicine, University College London Hospitals, 235  
48 Euston Rd, Fitzrovia, London, United Kingdom, NW1 2BU
- 49 15. Lungs for Living Research Centre. Division of Medicine, Rayne Building. University  
50 College London, 5 University Street. London. WC1E 6JF

- 51 16. Department of Radiology, University College London Hospitals, 235 Euston Rd,  
52 Fitzrovia, London, United Kingdom, NW1 2BU
- 53 17. Institute of Cancer Studies, University of Manchester, Oxford Road, Manchester, M13  
54 9PL
- 55 18. The Christie Hospital, Manchester, United Kingdom, M20 4BX
- 56 19. Department of Cardiothoracic Surgery, University Hospitals of South Manchester,  
57 Manchester, M23 9LT
- 58 20. Department of Pathology, University Hospitals of South Manchester, Manchester, M23  
59 9LT
- 60 21. North West Lung Centre, University Hospital of South Manchester, Manchester,  
61 United Kingdom, M23 9LT
- 62 22. Department of Thoracic Surgery, Birmingham Heartlands Hospital, Birmingham,  
63 United Kingdom, B9 5SS
- 64 23. Department of Medical Oncology, Birmingham Heartlands Hospital, Birmingham,  
65 United Kingdom, B9 5SS
- 66 24. Department of Cellular Pathology, Birmingham Heartlands Hospital, Birmingham,  
67 United Kingdom, B9 5SS
- 68 25. Department of Medical Oncology, Aberdeen University Medical School & Aberdeen  
69 Royal Infirmary, Aberdeen, Scotland, United Kingdom, AB25 2ZN
- 70 26. Department of Cardiothoracic Surgery, Aberdeen University Medical School &  
71 Aberdeen Royal Infirmary, Aberdeen, United Kingdom, AB25 2ZD
- 72 27. Department of Pathology, Aberdeen University Medical School & Aberdeen Royal  
73 Infirmary, Aberdeen, Scotland, United Kingdom, AB25 2ZD
- 74 28. Department of Respiratory Medicine, Aberdeen University Medical School &  
75 Aberdeen Royal Infirmary, Aberdeen, United Kingdom, AB25 2ZN

- 76 29. Department of Radiology, Aberdeen University Medical School & Aberdeen Royal  
77 Infirmary, Aberdeen, Scotland, United Kingdom, AB25 2ZN
- 78 30. Department of Thoracic Surgery, Glenfield Hospital, Leicester, LE3 9QP
- 79 31. Department of Radiotherapy, North Middlesex University Hospital, London N18 1QX
- 80 32. Department of Respiratory Medicine, Royal Free Hospital, Pond Street, London, NW3  
81 2QG
- 82 33. Department of Respiratory Medicine, Barnet and Chase Farm Hospitals, Wellhouse  
83 Lane, Barnet, United Kingdom, EN5 3DJ
- 84 34. Department of Respiratory Medicine, The Princess Alexandra Hospital, Hamstel Rd,  
85 Harlow CM20 1QX
- 86 35. Department of Clinical Oncology, St.Luke's Cancer Centre, Royal Surrey County  
87 Hospital, Guildford, GU2 7XX
- 88 36. Department of Pathology, Ashford and St. Peters' Hospital, Guildford Road, Chertsey,  
89 Surrey, KT16 0PZ
- 90 37. Department of Respiratory Medicine, Ashford and St. Peters' Hospital, Guildford Road,  
91 Chertsey, Surrey, KT16 0PZ
- 92 38. Department of Radiology, Ashford and St. Peters' Hospital, Guildford Road, Chertsey,  
93 Surrey, KT16 0PZ
- 94 39. Department of Clinical Oncology, Velindre Hospital, Cardiff, Wales, United Kingdom,  
95 CF14 2TL
- 96 40. Department of Cardiothoracic Surgery, University Hospital Llandough, Cardiff, Wales,  
97 United Kingdom, CF64 2XX
- 98 41. Department of Pathology, University Hospital Llandough, Cardiff, Wales, United  
99 Kingdom, CF64 2XX

- 100 42. Department of Radiology, University Hospital Llandough, Cardiff, Wales, United  
101 Kingdom, CF64 2XX
- 102 43. Department of Respiratory Medicine, University Hospital Llandough, Cardiff, Wales,  
103 United Kingdom, CF64 2XX
- 104 44. UCL ECMC GCLP Facility, University College London Cancer Institute, Paul  
105 O'Gorman Building, 72 Huntley Street, London, WC1E 6BT
- 106 45. Department of Respiratory Medicine, The Whittington Hospital NHS Trust, United  
107 Kingdom, N19 5NF
- 108 46. University College London, Cancer Research UK & UCL Cancer Trials Centre,  
109 London, United Kingdom, W1T 4TJ
- 110 47. Centre for Biological Sequence Analysis, Department of Systems Biology, Technical  
111 University of Denmark, 2800 Lyngby, Denmark.
- 112 48. Computational Health Informatics Program (CHIP), Boston Children's Hospital,  
113 Harvard Medical School, Boston, MA, USA.
- 114 49. MTA-SE-NAP, Brain Metastasis Research Group, 2nd Department of Pathology,  
115 Semmelweis University, 1091 Budapest, Hungary.
- 116 50. Berlin Institute for Medical Systems Biology, Max Delbrueck Center for Molecular  
117 Medicine, Berlin, Germany
- 118 51. Bill Lyons Informatics Centre, University College London Cancer Institute, Paul  
119 O'Gorman Building, 72 Huntley Street, London, WC1E 6BT
- 120 52. Department of Bioinformatics and Biostatistics, The Francis Crick Institute, 1 Midland  
121 Rd, London NW1 1AT
- 122 53. Cancer Immunology Unit, University College London Cancer Institute, Paul O'Gorman  
123 Building, 72 Huntley Street, London, WC1E 6BT

124 54. Cancer Genomics Laboratory, The Francis Crick Institute, 1 Midland Rd, London NW1  
125 1AT

126 55. Department of Human Genetics, University of Leuven, B-3000 Leuven, Belgium

127 56. Cancer Research UK Manchester Institute, Manchester, United Kingdom, M20 4BX

128 57. Dana-Farber Cancer Institute, 450 Brookline Ave. Boston, United States, MA 02215-  
129 5450

130

131 Corresponding author:

132 Charles Swanton

133 Translational Cancer Therapeutics Laboratory

134 The Francis Crick Institute

135 3rd Floor South West

136 1 Midland Road

137 London

138 NW1 1A

139 Email: [Charles.Swanton@crick.ac.uk](mailto:Charles.Swanton@crick.ac.uk)

140 Office +44 203 796 2047

141 **Summary (156 words)**

142 Earlier detection of relapse following primary surgery for non-small cell lung cancer and the  
143 characterization of emerging subclones seeding metastatic sites might offer new therapeutic  
144 approaches to limit tumor recurrence. The potential to non-invasively track tumor evolutionary  
145 dynamics in ctDNA of early-stage lung cancer is not established. Here we conduct a patient-  
146 specific approach to ctDNA profiling in the first 100 lung TRACERx (**TR**acking **C**ancer  
147 **E**volution through therapy (**R**x)) study participants, including one patient co-recruited to the  
148 PEACE (**P**osthumous **E**valuation of **A**dvanced **C**ancer **E**nvironment) post-mortem study. We  
149 identify independent predictors of ctDNA release in early-stage non-small cell lung cancer and  
150 perform tumor volume limit of detection analyses. Through blinded profiling of post-operative  
151 plasma, we observe evidence of adjuvant chemotherapy resistance and identify patients  
152 destined to experience recurrence of their lung cancer. Finally, we show that phylogenetic  
153 ctDNA profiling tracks the subclonal nature of lung cancer relapse and metastases, providing  
154 a new approach for ctDNA driven therapeutic studies

155

156

157 **Main text**

158 Lung cancer is the leading cause of cancer death worldwide<sup>1-2</sup>. Established metastatic non-  
159 small cell lung cancer (NSCLC) cannot be cured with systemic chemotherapy. Yet clinical  
160 studies have shown a 5% benefit of post-operative (adjuvant) chemotherapy on overall  
161 survival<sup>3</sup>. This modest survival benefit may reflect a vulnerability of treating low volume  
162 disease within the context of reduced intra-tumor heterogeneity<sup>4</sup>. Improving adjuvant treatment  
163 of lung cancer could improve cure rates. However, achieving this objective will require the  
164 development of a diagnostic platform capable of identifying, monitoring and genomically  
165 characterizing recurring or residual disease early. This would create a therapeutic setting where  
166 only patients destined to recur would receive treatment, where intervention could be directed  
167 to the evolving tumor subclone seeding metastatic recurrence guided by clinical trials powered  
168 to determine treatment effect within smaller patient cohorts.

169 Circulating tumor DNA (ctDNA) detection in plasma has been shown in breast<sup>5,6</sup> and colorectal  
170 cancer<sup>7</sup> to detect minimal residual disease in the adjuvant setting and identify patients destined  
171 to relapse post-operatively in advance of established clinical parameters. Here, we report a  
172 bespoke multiplex-PCR NGS approach to ctDNA profiling within the context of the



173 prospective tumor evolutionary NSCLC study TRACERx. We address determinants of ctDNA  
174 detection in early-stage NSCLC and investigate the ability of ctDNA to identify and  
175 genomically characterize, at subclone resolution, post-operative NSCLC relapse using a tumor  
176 phylogenetic framework.

### 177 **Phylogenetic ctDNA profiling**

178 The TRACERx study monitors the clonal evolution of NSCLC from diagnosis through to  
179 relapse and death<sup>8</sup>. Using multi-region exome sequencing (M-Seq) derived tumor phylogenetic  
180 trees developed through prospective analysis of the 100 patient TRACERx cohort, we  
181 conducted a phylogenetic approach to ctDNA profiling in early stage NSCLC (**Fig. 1**). Bespoke  
182 multiplex-PCR assay-panels were synthesised for each patient, targeting clonal and subclonal  
183 single nucleotide variants (SNVs) selected to track phylogenetic tumor branches in plasma (**Fig**  
184 **1**). Analytical validation of the multiplex-PCR NGS platform demonstrated a sensitivity of  
185 above 99% for the detection of SNVs at frequencies above 0.1% and the specificity of detecting  
186 a single SNV was 99.6% (**Extended Data Fig 1a**). At least two SNVs were detected in ctDNA  
187 from each NSCLC analyzed in our published discovery cohort data<sup>9</sup>, demonstrating biological  
188 sensitivity of a two SNV threshold for ctDNA detection in early-stage NSCLC. Therefore, we

189 prospectively selected a threshold of two detected SNVs for calling a sample ctDNA positive  
190 for validation within this study - to minimize type I error in a platform testing up to 30 tumour-  
191 specific SNVs per time-point in a single patient (see **Extended Data Fig 1b** for justification).  
192 Cross-platform validation was performed in 28 patients with M-Seq confirmed SNV(s) within  
193 one or more hotspots targeted by a generic multiplex PCR-NGS panel (**Extended Table 1a-b,**  
194 **Supplementary Table 1**). All 18 bespoke-panel ctDNA negative patients had no tumor SNVs  
195 detectable in plasma pre-operatively by the generic panel supporting biological specificity of  
196 the targeted approach, 7 of 10 bespoke-panel ctDNA positive patients had tumor SNVs  
197 detected in plasma by the generic panel (**Extended Table 1a-b**).

#### 198 **Determinants of ctDNA detection in NSCLC**

199 We sought to identify clinicopathological determinants of ctDNA detection in early-stage  
200 NSCLC by profiling pre-operative plasma samples in 96 of 100 TRACERx patients (cohort,  
201 sample characteristics **Extended Table 2a-c, Supplementary Table 2**). It was not possible to  
202 analyze samples from four patients (see **Extended Data Fig 2a** for details). Individual patient  
203 assay-panels were designed to target a median of 18 SNVs (range 10 to 22) comprising a

204 median of 11 clonal SNVs (range 2 to 20) and a median of 6 subclonal SNVs (range 0 to 16)  
205 **(Extended Data Fig 2b).**

206 At least two SNVs were detected in ctDNA pre-operatively in 46 of 96 (48%) early-stage  
207 NSCLCs, a single SNV was detected in 12 additional cases **(Fig 2a)**. Centrally reviewed  
208 pathological data revealed that ctDNA detection was associated with histological subtype: 97%  
209 (30/31) of lung squamous cell carcinomas (LUSCs) and 71% (5 of 7) of other NSCLC subtypes  
210 were ctDNA positive, compared with 19% (11/58) of lung adenocarcinomas (LUADs) **(Fig**  
211 **2a)**. ctDNA detection stratified by TNM stage revealed that 94% (16 of 17) of stage I LUSCs  
212 were detected compared with 13% (5 of 39) of stage I LUADs **(Extended Data Fig 3a)**.

213 Passive release of ctDNA into the circulation may be associated with apoptosis and necrosis<sup>10</sup>.

214 As expected<sup>11</sup>, LUSCs were significantly more necrotic than LUADs and ctDNA positive  
215 LUADs formed a sub-group of more necrotic tumors compared with ctDNA negative LUADs

216 **(Extended Data Fig 3b)**. Necrosis, lymph node involvement, lymphovascular invasion,

217 pathological tumor size, Ki67 labelling indices, non-adenocarcinoma histology and total cell-

218 free DNA input predicted ctDNA detection in univariable analyses **(Extended Data Fig 3c)**.

219 Multivariable analysis revealed non-adenocarcinoma histology, the presence of lympho-

220 vascular invasion and high Ki67 proliferation index as independent predictors of ctDNA

221 detection (**Extended Data Fig 3c**). Since FDG-avidity on positron emission tomography (PET)  
222 scans correlates with proliferative indices in early-stage NSCLC<sup>12,13</sup>, we investigated tumor  
223 PET FDG-avidity and ctDNA detection. PET FDG-avidity predicted ctDNA detection (area  
224 under curve = 0.84, P<0.001, n=92) (**Extended Data Fig 3d**). Within LUADs, common driver  
225 events in *KRAS*, *EGFR* or *TP53* were not associated with ctDNA detection (**Extended Data**  
226 **Fig 3e**).

227 We analyzed the distribution of clonal and subclonal SNVs in ctDNA positive patients. Clonal  
228 SNVs were detected in all 46 ctDNA positive patients; a median of 94% (range 11% to 100%)  
229 of clonal SNVs targeted by assay-panels were detected in ctDNA. 40 of 46 ctDNA positive  
230 patients had subclonal SNVs targeted by assay-panels and subclonal SNVs were detected in 27  
231 (68%) of these patients. A median of 27% (range 0% to 91%) of targeted subclonal SNVs were  
232 detected in ctDNA positive patients (**Figure 2b**). The mean plasma variant allele frequency  
233 (VAF) of clonal SNVs was significantly higher than that of subclonal SNVs (**Extended Data**  
234 **Fig 4a**) (within patient comparison, Wilcoxon signed-rank test, P<0.001, n=27,  
235 **Supplementary Table 3**) supporting the use of clonal alterations as a more sensitive method  
236 of ctDNA detection than subclonal alterations<sup>9,14</sup>.

237 In ctDNA positive patients, macroscopic tumor size correlated with mean clonal plasma VAF  
238 (Spearman's  $Rho = 0.405$ ,  $P=0.005$ ,  $n=46$ ) (**Extended Data Fig 4b**). CT scan volumetric  
239 analyses were available in 38 of 46 ctDNA positive patients (see **Extended Data Fig 4c**).  
240 Tumor volume correlated with mean clonal plasma VAF (**Fig 3a**, Spearman's  $Rho = 0.61$ ,  
241  $P<0.001$ ,  $n=38$ ). A linear relationship between log- transformed volume and mean clonal VAF  
242 values was observed (**Fig 3a**). The line of best fit applied to our data was consistent with the  
243 line fitted to NSCLC volumetric data and ctDNA plasma VAFs reported in previously  
244 published work<sup>15</sup> (**Extended Data Fig 4d**). Linear modelling based on the TRACERx data  
245 approximated that a primary tumor volume of  $11\text{cm}^3$  would result in a mean clonal plasma  
246 VAF of 0.1% (**Figure 3b**). We multiplied tumor purity by tumor volume to control for stromal  
247 contamination and determine cancer cell volume (**Extended Data Fig 4e**). On the assumption  
248 that  $1\text{cm}^3$  of effective tumor contains  $9.4 \times 10^7$  cells we approximated that a plasma VAF of  
249 0.1% corresponds to a tumor burden of 326 million malignant cells (**Extended Data Fig 4f**).  
250 To investigate predictors of subclone detection we mapped detected subclonal SNVs back to  
251 M-seq derived tumor phylogenetic trees. 35 of 57 (61%) shared subclones (identified in more  
252 than one tumor region through M-Seq analysis) were identified in ctDNA, compared with 26  
253 of 80 (33%) private subclones (detected in a single tumor region only) (**Extended Data Fig**

254 **4g**). This suggested subclone volume influences subclonal ctDNA detection. We estimated  
255 subclone volume based on mean regional subclone cancer cell fraction (CCF) and cancer cell  
256 volume. Detected subclonal SNVs mapped to subclones with significantly higher estimated  
257 volumes than subclones containing undetected SNVs (**Figure 3c**) and subclone volume  
258 correlated with subclonal SNV plasma VAF (**Figure 3d**).

### 259 **Detecting and characterizing NSCLC relapse**

260 The longitudinal phase of the study aimed to determine if ctDNA profiling with patient-specific  
261 assay panels could detect and characterize the branched subclone(s) seeding NSCLC relapse.  
262 Pre- and post-surgical plasma ctDNA profiling was performed blinded to relapse status in a  
263 sub-group of 24 patients (cohort characteristics, **Extended Table 2d-e**). This included relapse  
264 free patients who had been followed-up for a median of 775 days (range 688 to 945 days, n=10)  
265 and confirmed NSCLC relapse cases (n=14) (cohort design, **Extended Data Fig 2c**). PCR  
266 assays were added to panels in this phase of the study to optimize sensitivity in LUADs. A  
267 median of 18.5 SNVs (range 12 to 20) were targeted by LUSC assay-panels and a median of  
268 28 SNVs (range 25 to 30) were targeted by LUAD assay-panels (**Extended Data Fig 2d-e**).

269 Patients were followed up with three to six monthly clinical assessment and chest radiographs.

270 At least 2 SNVs were detected in 13 of 14 (93%) patients with confirmed NSCLC relapse prior

271 to, or at, clinical diagnosis of relapse and detected in 1 of 10 (10%) patients (CRUK0013) with

272 no clinical evidence of NSCLC relapse (**Fig 4a-k, Extended Data Fig 5a-n**). Excluding a

273 single case where no post-operative plasma was taken prior to clinical relapse (CRUK0041)

274 the median interval between ctDNA detection and NSCLC relapse confirmed on clinically

275 indicated CT imaging (lead-time) was 70 days (range 10 to 346 days). Four of 13 relapse cases

276 exhibited lead-times of more than six months (**Fig 4a-d**). In two cases ctDNA detection

277 preceded CT imaging inconclusive for NSCLC relapse by 347 days (**Fig 4a**) and 260 days (**Fig**

278 **4d**). Post-operative ctDNA profiling reflected adjuvant chemotherapy resistance; CRUK0004,

279 CRUK0080 and CRUK0062 had detectable ctDNA in plasma within 30 days of surgery. The

280 number of detectable SNVs increased in all cases despite adjuvant chemotherapy with disease

281 recurring within 1 year of surgery (**Fig. 4a-c**). In contrast, CRUK0013 had 20 SNVs detectable

282 in ctDNA 72 hours after surgery and 13 SNVs detectable prior to adjuvant chemotherapy (**Fig**

283 **4e**). 51 days following completion of adjuvant treatment, no SNVs were detectable. Two

284 further plasma samples were profiled for this patient at day 457 and 667; ctDNA remained

285 undetectable and the patient remains relapse free 688 days post-surgery (**Fig 4e**). ctDNA

286 profiling detected intracerebral relapse; CRUK0029 had a pre-operative PET scan performed  
287 50 days prior to surgery demonstrating normal cerebral appearances. Mean clonal plasma VAF  
288 of detected SNVs remained above 1% 30 days post-surgery, 54 days post-operatively the  
289 patient was confirmed to have intracerebral metastasis (**Fig 4f**).

290 We sought to resolve subclonal evolutionary-dynamics associated with NSCLC relapse.  
291 Subclonal SNVs displaying plasma VAFs similar to clonal SNVs and mapping to phylogenetic  
292 clusters confined to a single phylogenetic branch, were detected post-operatively in the ctDNA  
293 of four patients who suffered NSCLC relapse (CRUK0004, CRUK0063, CRUK0065 and  
294 CRUK0044) (**Fig. 4a,g-i**). These findings suggested a relapse process dominated by a subclone  
295 represented in our assay-panel. Notably the subclone implicated by ctDNA as driving the  
296 relapse in the case of CRUK0004 contained an ERBB2 (HER2) amplification event that may  
297 be targetable in NSCLC<sup>16</sup>. This suggests ctDNA defined subclonal evolution may inform  
298 precision strategies against emerging subclones (**Fig. 4a**). Relapses involving subclones from  
299 more than one phylogenetic branch were evident in patients CRUK0080, CRUK0062 and  
300 CRUK0041 (**Fig 4b-c,j**).

### 301 **Validation of phylogenetic characterization**



302 To validate subclonal ctDNA analyses, data acquired from sequencing metastatic tissue was  
303 interpreted with M-seq primary tumor data (**Supplementary Table 4**). Patient CRUK0063  
304 suffered para-vertebral relapse of their NSCLC. Post-operative ctDNA analysis revealed the  
305 detection of the same subclonal SNV (*OR5D18*) on four consecutive occasions over a 231-day  
306 period (**Extended Data Fig 6a**). The *OR5D18* SNV traced back to a subclonal cluster private  
307 to primary tumor region three (**Fig 5a**). Exome sequencing of CT-guided biopsy tissue acquired  
308 from the para-vertebral metastasis revealed the subclone implicated in the metastatic event by  
309 detection of the *OR5D18* SNV in ctDNA gave rise to the metastatic clone. This supported  
310 ctDNA phylogenetic characterization of relapse (**Fig 5a**). The para-vertebral biopsy contained  
311 88 SNVs not present in the primary tumor including an *ARID1A* stop-gain driver SNV. Re-  
312 examination of primary tumor region M-Seq data with a lower SNV calling threshold revealed  
313 that 16 of 88 SNVs including *ARID1A* were detectable in primary tumor region three, compared  
314 to a maximum of 2 of 88 in other tumor regions (**Extended Data Fig 6b**). Since ctDNA  
315 implicated the subclone private to primary tumor region three in the relapse process, these data  
316 suggest that ctDNA profiling can resolve the primary tumor region from which a low frequency  
317 metastatic subclone derives. CRUK0035 developed two liver and one adrenal metastases (**Fig**  
318 **5b**). Sequencing of the metastatic liver deposit revealed that only 109 of 149 SNVs classed as

319 clonal in the primary tumor were detectable in the metastasis. This was suggestive of an  
320 ancestral branching event not resolved through primary M-seq analysis (**Figure 5b**). Post-  
321 operative ctDNA profiling identified clonal SNVs present in the liver metastasis biopsy but  
322 also revealed SNVs representing a subclone from the primary tumor (**Extended Data Fig 6c**).  
323 This subclone was not present in the metastatic liver deposit (**Fig 5b**). These data may reflect  
324 ctDNA identified from the non-biopsied metastases suggesting multiple metastatic events.  
325 CRUK0044 suffered a vertebral and right hilar relapse. Post-operatively the same subclonal  
326 SNV (*OR10K1*), was detected in ctDNA on two occasions 85 days apart (**Extended Data Fig**  
327 **6d**). This SNV represented a single subclone detected through sequencing hilar lymph-node  
328 metastatic tissue, supporting ctDNA findings (**Fig. 5c**). CRUK0041 suffered an intracerebral,  
329 hilar and subcarinal lymph node relapse. Four subclonal SNVs representing both branches of  
330 the tumor phylogenetic tree were detectable in ctDNA at relapse. Concordant with these data,  
331 sequencing of subcarinal metastatic tissue revealed the presence of subclonal SNVs mapping  
332 to both phylogenetic branches (**Fig 5d, Extended Data Fig. 6e**). Patient CRUK0013 was found  
333 to have lymph-node metastases following primary surgery. Two lymph node metastases were  
334 sampled for exome analysis together with M-seq of the primary tumor. Subclonal SNVs  
335 detected in ctDNA post-operatively mapped to an ancestral subclone (describing a subclone

336 that existed during the tumor's evolution) containing a KRAS amplification (**Extended Data**  
337 **Fig 6f, Fig. 5e**). This ancestral subclone was present in the primary tumor and sampled lymph-  
338 nodes (**Fig. 5e**). Given the lymph node involvement in this case these findings suggest residual  
339 metastatic lymphadenopathy following surgery that responded to adjuvant chemoradiotherapy  
340 (**Fig. 4e**)

#### 341 **ctDNA profiling in the metastatic setting**

342 Patient CRUK0063 underwent examination through the PEACE post-mortem study 24 hours  
343 following death. Six tumor regions were sampled from three metastatic sites (thoracic  
344 vertebral, para-aortic and lung metastases). M-Seq data from the six post-mortem tumor  
345 regions (day 857), the para-vertebral relapse biopsy (day 467) and five primary tumor regions  
346 (day 0) were combined to infer the phylogenetic structure of this patient's NSCLC (**Fig 6a**).  
347 All seven metastatic tumor regions arose from a single ancestral subclone represented by  
348 phylogenetic cluster 8 (**Fig 6b**). Six metastatic regions shared a later phylogenetic origin,  
349 phylogenetic cluster 12 (**Fig. 6b**). The single tumor region that had not arisen from  
350 phylogenetic cluster 12 was sampled from the para-aortic metastasis at autopsy and contained  
351 a private subclone represented by phylogenetic cluster 9 (**Fig 6b**). The findings could represent

352 two or more independent metastatic events arising from a single branch of the primary tumor  
353 phylogenetic tree, with ongoing tumor evolution at each metastatic site (**Fig 6b**). Or a single  
354 metastatic event to the para-aortic site involving the ancestral subclone (phylogenetic cluster  
355 8) prior to evolution of the subclone represented by phylogenetic cluster 9. Followed by  
356 metastatic cross-seeding to para-vertebral and lung sites and ongoing clonal evolution (**Fig 6b**).

357 We designed a bespoke ctDNA assay-panel to retrospectively track metastatic subclonal  
358 burden. 20 clonal SNVs and a median of 8 subclonal SNVs (range 4 to 15) in 9 metastatic  
359 subclonal clusters were targeted by the assay-panel (**Extended Data Fig 7**). Since 103 variants  
360 per time-point were profiled, SNV call thresholds were increased to maintain platform  
361 specificity of more than 99.2% at the 2 SNV ctDNA detection threshold (see **Extended**  
362 **Methods**). ctDNA detection occurred at day 340 post-surgery (**Fig 6c, Extended Data Fig 7**).

363 At day 466 following clinical-relapse at the thoracic para-vertebral site, 18 of 20 SNVs  
364 mapping to phylogenetic clusters (8,11 and 12) were detected in ctDNA (**Fig 6c, Extended**  
365 **Data Fig 7**). These subclonal clusters were shared between six of seven metastatic sites (**Fig**  
366 **6b**). A single SNV from a private subclone (phylogenetic cluster 9) was also detectable in  
367 ctDNA at day 466 (**Fig 6c, Extended Data Fig 7**). This subclone was not identified in the CT  
368 guided para-vertebral biopsy taken at day 467 (**Fig 6b**). The mean plasma VAF of the 18 SNVs

369 detected in phylogenetic clusters 11, 8 and 12 reflected their proximity to the clonal cluster  
370 (light blue) in the M-Seq derived phylogenetic tree (**Fig 6c**). This suggested a tiered burden of  
371 subclonal disease concordant with M-seq phylogenetic inferences (**Fig 6a**). Mean clonal VAF  
372 fell in response to palliative radiotherapy and chemotherapy but at day 767 increased (**Fig 6c**).  
373 Single SNVs mapping to phylogenetic clusters 5 and 9 and two SNVs mapping to phylogenetic  
374 cluster 2 were now detectable in ctDNA 90 days before death (**Fig 6a-c, Extended Data Fig**  
375 **7**). These phylogenetic clusters represented subclones private to the para-aortic metastases (**Fig**  
376 **6a-b**). Consistent with these data significant para-aortic progression was observed at post-  
377 mortem compared with most recent CT imaging performed 112 days before death - which  
378 showed no evidence of para-aortic disease.

## 379 **Discussion**

380 In summary, we find predictors of ctDNA detection in early-stage NSCLC characterized by  
381 non-adenocarcinoma histology, necrosis, increased proliferative indices and lymphovascular  
382 invasion (**Fig 2a**). Triple negative breast cancers display necrosis<sup>17</sup>, high proliferative  
383 indices<sup>18,19</sup> and are associated with increased ctDNA levels compared with other breast cancer  
384 subtypes<sup>6</sup> suggesting extension of observations to other tumor types.

385 We find a relationship between tumor volume and ctDNA detection. We estimate that a primary  
386 NSCLC tumor with a volume of  $11\text{cm}^3$  is required to achieve a ctDNA plasma VAF of 0.1%  
387 (**Fig. 3b**), a VAF reflecting the optimum sensitivity of most current ctDNA platforms. Low-  
388 dose CT lung screening can identify lung nodules with diameters as low as  $4\text{mm}^{20}$ . Assuming  
389 a spherical nodule, this would translate to a volume of  $0.034\text{cm}^3$  and an approximate plasma  
390 VAF of  $1.4 \times 10^{-4} \%$  - at the extreme of detection limits of ctDNA platforms<sup>21</sup>. Sensitivity of  
391 ctDNA NSCLC screening may therefore be constrained by tumor size using current  
392 technologies. ctDNA release dynamics may alter at disease relapse - in three LUAD cases we  
393 detect no ctDNA pre-operatively, yet detect ctDNA at relapse in the absence of clinically  
394 detectable disease (**Fig 4a,d,i**).

395 Targeted ctDNA profiling characterized the subclonal dynamics of relapsing NSCLC.  
396 Limitations to this approach include cost, estimated at \$1750 per patient for single region tumor  
397 sequencing with evaluation of five plasma samples and synthesis of bespoke assay-panels  
398 within a clinically relevant timeframe. Adjuvant platinum-based chemotherapy in NSCLC  
399 improves cure rates following surgery in only 5% of patients and 20% patients receiving  
400 chemotherapy experience acute toxicities<sup>22</sup>. There is an urgent need to increase adjuvant  
401 therapy efficacy and better target its use. Our findings indicate that drug development guided

402 by ctDNA platforms to identify residual disease, define treatment response and target emerging  
403 subclones in the adjuvant NSCLC setting, with appropriate CLIA validation, are now feasible.

## 404 **References**

- 405
- 406
- 407 1. Jemal A, Bray F, Center MM, Ferlay J, Ward E, Forman D. Global cancer statistics. *CA: A*  
408 *Cancer Journal for Clinicians* 2011;61(2):69-90.
- 409 2. Siegel RL, Miller KD, Jemal A. Cancer statistics, 2017. *CA: A Cancer Journal for Clinicians*  
410 2017;67(1):7-30.
- 411 3. Pignon J-P, Tribodet H, Scagliotti GV, Douillard J-Y, Shepherd FA, Stephens RJ, et al. Lung  
412 Adjuvant Cisplatin Evaluation: A Pooled Analysis by the LACE Collaborative Group. *Journal of*  
413 *Clinical Oncology* 2008;26(21):3552-9.
- 414 4. Landau Dan A, Carter Scott L, Stojanov P, McKenna A, Stevenson K, Lawrence Michael S, et  
415 al. Evolution and Impact of Subclonal Mutations in Chronic Lymphocytic Leukemia.  
416 *Cell*;152(4):714-26.
- 417 5. Beaver JA, Jelovac D, Balukrishna S, Cochran RL, Croessmann S, Zabransky DJ, et al. Detection  
418 of Cancer DNA in Plasma of Patients with Early-Stage Breast Cancer. *Clinical Cancer Research*  
419 2014;20(10):2643-50.
- 420 6. Garcia-Murillas I, Schiavon G, Weigelt B, Ng C, Hrebien S, Cutts RJ, et al. Mutation tracking in  
421 circulating tumor DNA predicts relapse in early breast cancer. *Science Translational Medicine*  
422 2015;7(302):302ra133-302ra133.
- 423 7. Tie J, Wang Y, Tomasetti C, Li L, Springer S, Kinde I, et al. Circulating tumor DNA analysis  
424 detects minimal residual disease and predicts recurrence in patients with stage II colon  
425 cancer. *Science Translational Medicine* 2016;8(346):346ra92-ra92.
- 426 8. Jamal-Hanjani M, Hackshaw A, Ngai Y, Shaw J, Dive C, Quezada S, et al. Tracking genomic  
427 cancer evolution for precision medicine: the lung TRACERx study. *PLoS Biol*  
428 2014;12(7):e1001906.
- 429 9. Jamal-Hanjani M, Wilson GA, Horswell S, Mitter R, Sakarya O, Constantin T, et al. Detection  
430 of ubiquitous and heterogeneous mutations in cell-free DNA from patients with early-stage  
431 non-small-cell lung cancer. *Annals of Oncology* 2016;27(5):862-7.
- 432 10. Jr LAD, Bardelli A. Liquid Biopsies: Genotyping Circulating Tumor DNA. *Journal of Clinical*  
433 *Oncology* 2014;32(6):579-86.
- 434 11. Caruso R, Parisi A, Bonanno A, Paparo D, Quattrocchi E, Branca G, et al. Histologic  
435 coagulative tumour necrosis as a prognostic indicator of aggressiveness in renal, lung,  
436 thyroid and colorectal carcinomas: A brief review. *Oncology Letters* 2012;3(1):16-8.
- 437 12. Vesselle H, Schmidt RA, Pugsley JM, Li M, Kohlmyer SG, Vallières E, et al. Lung Cancer  
438 Proliferation Correlates with [F-18]Fluorodeoxyglucose Uptake by Positron Emission  
439 Tomography. *Clinical Cancer Research* 2000;6(10):3837-44.
- 440 13. Higashi K, Ueda Y, Yagishita M, Arisaka Y. FDG PET measurement of the proliferative  
441 potential of non-small cell lung cancer. *The Journal of Nuclear Medicine* 2000;41(1):85.
- 442 14. Murtaza M, Dawson S-J, Pogrebniak K, Rueda OM, Provenzano E, Grant J, et al. Multifocal  
443 clonal evolution characterized using circulating tumour DNA in a case of metastatic breast  
444 cancer. *Nature Communications* 2015;6:8760.
- 445 15. Newman AM, Bratman SV, To J, Wynne JF, Eclow NCW, Modlin LA, et al. An ultrasensitive  
446 method for quantitating circulating tumor DNA with broad patient coverage. *Nat Med*  
447 2014;20(5):548-54.

- 448 16. Peters S, Zimmermann S. Targeted therapy in NSCLC driven by HER2 insertions. *Translational Lung Cancer Research* 2014;3(2):84-8.
- 449
- 450 17. Livasy CA, Karaca G, Nanda R, Tretiakova MS, Olopade OI, Moore DT, et al. Phenotypic  
451 evaluation of the basal-like subtype of invasive breast carcinoma. *Mod Pathol*  
452 2005;19(2):264-71.
- 453 18. Keam B, Im S-A, Kim H-J, Oh D-Y, Kim JH, Lee S-H, et al. Prognostic impact of  
454 clinicopathologic parameters in stage II/III breast cancer treated with neoadjuvant docetaxel  
455 and doxorubicin chemotherapy: paradoxical features of the triple negative breast cancer.  
456 *BMC Cancer* 2007;7:203-.
- 457 19. Rhee J, Han SW, Oh DY, Kim JH, Im SA, Han W, et al. The clinicopathologic characteristics and  
458 prognostic significance of triple-negativity in node-negative breast cancer. *BMC Cancer*  
459 2008;8:307.
- 460 20. Team TNLSTR. Reduced Lung-Cancer Mortality with Low-Dose Computed Tomographic  
461 Screening. *New England Journal of Medicine* 2011;365(5):395-409.
- 462 21. Newman AM, Lovejoy AF, Klass DM, Kurtz DM, Chabon JJ, Scherer F, et al. Integrated digital  
463 error suppression for improved detection of circulating tumor DNA. *Nat Biotech*  
464 2016;34(5):547-55.
- 465 22. Pignon JP, Tribodet H, Scagliotti GV, Douillard JY, Shepherd FA, Stephens RJ, et al. Lung  
466 adjuvant cisplatin evaluation: a pooled analysis by the LACE Collaborative Group. *J Clin Oncol*  
467 2008;26(21):3552-9.

468

469 **Supplementary information** is available in the online version of the paper

470 **Acknowledgements** We dedicate this manuscript to the memory of Roberto Macina. We also  
471 thank Samantha Navarro and Antony Tin for facilitating the PEACE ctDNA analysis presented  
472 in this manuscript. We thank the members of the TRACERx and PEACE consortia (see  
473 Supplementary Appendix for a list of centres and investigators) for participating in this study.  
474 C.S. is Royal Society Napier Research Professor. This work was supported by the Francis Crick  
475 Institute which receives its core funding from Cancer Research UK (FC001169), the UK  
476 Medical Research Council (FC001169), and the Wellcome Trust (FC001169 ); by the UK  
477 Medical Research Council (grant reference MR/FC001169 /1); CS is funded by Cancer  
478 Research UK (TRACERx and CRUK Cancer Immunotherapy Catalyst Network), the CRUK  
479 Lung Cancer Centre of Excellence, Stand Up 2 Cancer (SU2C), the Rosetrees Trust,  
480 NovoNordisk Foundation (ID 16584), the Prostate Cancer Foundation, the Breast Cancer  
481 Research Foundation, the European Research Council (THESEUS) and Support was provided



482 to CS by the National Institute for Health Research, the University College London Hospitals  
483 Biomedical Research Centre, and the Cancer Research UK University College London  
484 Experimental Cancer Medicine Centre.

485 **Authorship contribution statement**

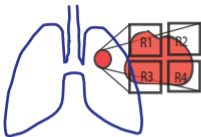
486 C.A., N.J.B., G.A.W., M.J.H., T.C., R.S., and J.L-Q. contributed equally to this work. C.A.  
487 and C.S. co-wrote the manuscript. C.A., M.J.H., and C.S. conceived study design. C.A., N.J.B.,  
488 G.A.W. and R.R. integrated clinicopathological data, exome data and multiplex-PCR NGS  
489 data. B.G.Z, J.L., T.C., R.S., E.K., N.S., D.H., A.N. and A.P., conducted and analysed  
490 multiplex-PCR NGS experimental work. N.J.B, G.A.W, T.B.K.W, R.R., and N.M. conducted  
491 bioinformatic analyses of TRACERx data. J.L-Q and D.A.M. conducted a central pathological  
492 review. T.M. analyzed tissue micro-array data. F.F., R.E. and F.Z. conducted central  
493 radiological review of pre-operative PET scans. H.J.W.L.A., W.L.B., F.M.F. and N.J.B.  
494 conducted volumetric analyses of pre-operative CT scans. S.V., D.J., J.L., S.S., J.C-K., A.R.,  
495 T.C., D.O. and A.A. conducted technical work for TRACERx sample processing. G.E., S.W.,  
496 N.M. and G.A.W. conducted TRACERx sample exome sequencing. L.M. and J.R. conducted  
497 cross-platform validation on TRACERx cell-free DNA samples. M.J.H., C.S. and M.Fa.  
498 designed the PEACE protocol. M.J.H., C.D., J.S. and C.S. designed the TRACERx protocol.  
499 C.H., S.L.M., M.F., T.A., M.Fa., E.B., D.L., M.H., S.K., N.P., S.M.J., R.T., A.A., F.B., Y.S.,  
500 R.S., L.J., A.M.Q, P.C., B.N., G.M., G.L., S.T., M.N., H.R., K.K., M.C., L.G., D.F., A.N., S.R.,  
501 G.A., S.K., P.R., V.E., B.I., M.I-S., V.P., J.L., M.K., R.A., H.A., H.D., S.L. are integral clinical  
502 members of TRACERx study sites. J.H. and H.L. run the UCL GCLP facility. A.H., H.B., N.I.  
503 and Y.N. were involved in study oversight. J.A.S., J.L-Q, Z.S., E.G., S.K., S.T., M.A.B, R.F.S.,  
504 J.H., A.S., S.Q., P.V.L., C.D. and J.L. gave advice and reviewed the manuscript. A.H. gave  
505 statistical advice. C.S. provided overall study oversight.

506 **Author information**

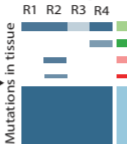
507 The authors declare competing financial interests. Reprints and permissions information is  
508 available at [www.nature.com/reprints](http://www.nature.com/reprints). Correspondence should be addressed to C.S.  
509 ([Charles.Swanton@crick.ac.uk](mailto:Charles.Swanton@crick.ac.uk)).

510

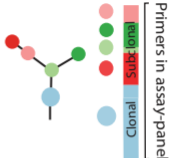
Primary NSCLC resection and multiregion sampling



Exome sequencing of tumor regions

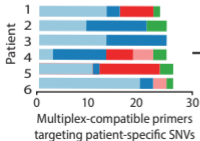


Phylogenetic tree informs PCR-assay panel construction



Multiple patient-specific assay panels combined

Multiplex-PCR assay-pool



Blood sample



PCR-NGS

Patient-specific phylogenetic tracking

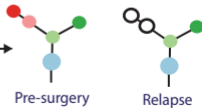


## **Figure 1 Phylogenetic ctDNA tracking**

Overview of the study methodology. Multi-region sequencing of Stage I-IIIb non-small cell lung cancers was performed through the TRACERx study. Phylogenetic trees were constructed. PCR assay-panels were designed targeting clonal and subclonal single nucleotide variants to facilitate non-invasive tracking of the patient-specific tumor phylogeny. Based on predicted and validated primer compatibility assay-panels were combined into multiplex assay-pools containing primers from up to 10 patients. Cell-free DNA was extracted from pre and post-operative plasma samples and multiplex-PCR performed. This was followed by next generation sequencing of amplicons. Findings were integrated with M-Seq exome data to track tumor evolution.

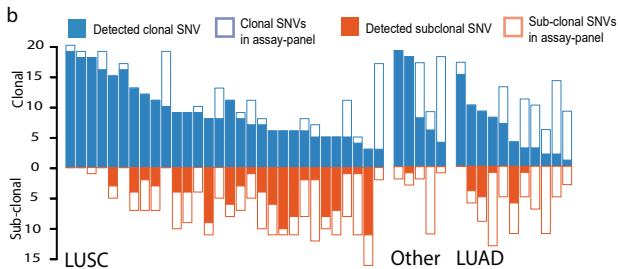
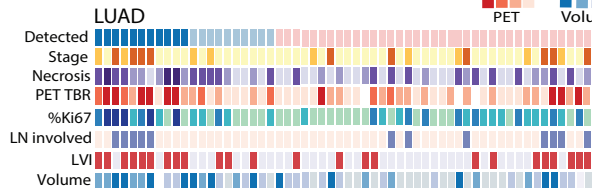
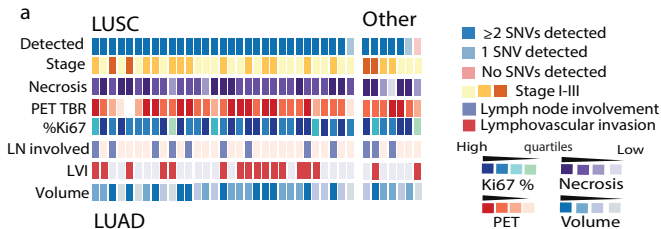


## **Figure 2 – Clinicopathological predictors of ctDNA detection**

a) Heatmap showing clinicopathological and ctDNA detection data, continuous variables quartiled. Raw data and patient IDs in Supplementary Table 1. b) Detection of clonal and subclonal single nucleotide variants within 46 patients with two or more single nucleotide variants detected in plasma. Histology indicated in panels as LUSC, LUAD and Other. Other histology refers to large cell carcinoma (1/1 ctDNA positive), adenosquamous carcinoma (2/3 ctDNA positive), large cell neuroendocrine carcinoma (1/1 ctDNA positive) and carcinosarcoma (1/2 ctDNA positive).

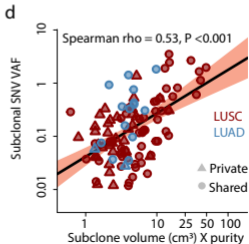
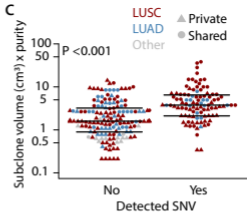
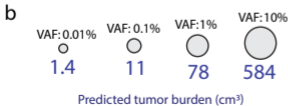
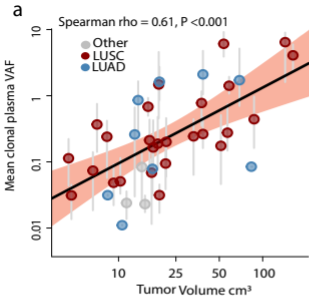


### **Figure 3. Tumor volume predicts plasma variant allele frequency**

a) Tumor volume ( $\text{cm}^3$ ) measured by CT volumetric analysis correlates with mean clonal plasma VAF,  $n=38$ , grey vertical lines represent range of clonal VAF, line of best fit estimated in log-space, 95% confidence intervals indicated by red shading. b) Predicted tumor burden at hypothetical clonal VAF intervals ranging from 0.01% to 10% based on linear model shown in panel a. c) Estimated effective subclone size, defined as mean CCF of subclone across sampled tumor regions multiplied by effective tumor volume (volume  $\times$  purity), influences subclonal SNV detection. For negative calls, median effective subclone size was  $1.60 \text{ cm}^3$ , range = 0.21-14.11,  $n=163$  for positive calls, median effective subclone size =  $3.97 \text{ cm}^3$ , range = 0.33 – 45.09,  $n=109$ . Wilcoxon rank sum test,  $P<0.001$ , data from 34 patients (who passed volumetric filters and had subclonal SNVs represented in assay-panel). d) Estimated effective subclone size correlates with subclonal plasma VAF,  $n=109$  subclonal SNVs, data from 24 patients (who passed volumetric filters with detected subclonal SNVs in plasma).



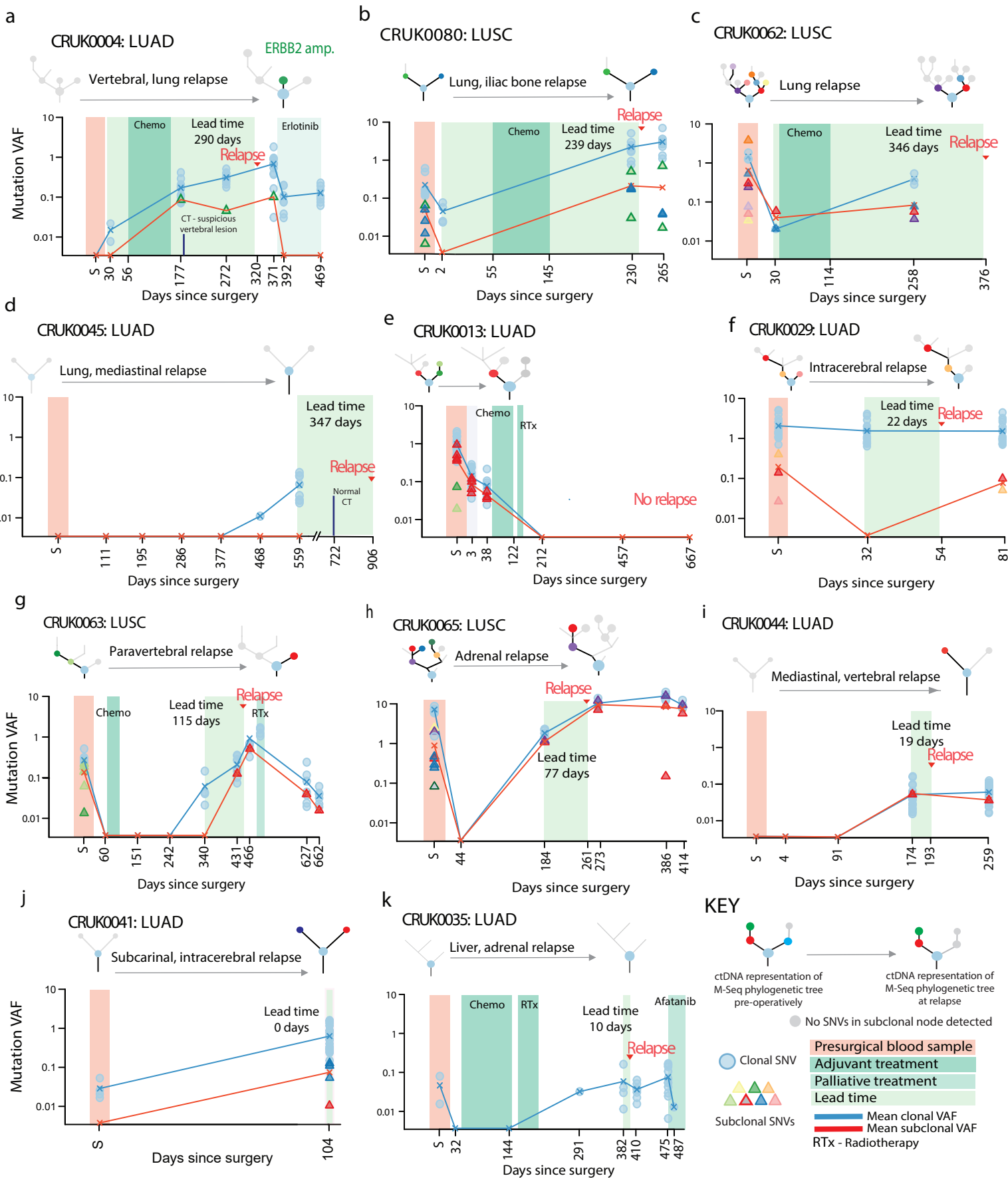


**Figure 4 – Post-operative ctDNA detection predicts and characterizes NSCLC relapse – 2a-k)** Longitudinal cell-free DNA profiling. Circulating tumor DNA (ctDNA) detection in plasma was defined as the detection of two tumor-specific SNVs. Relapse was based on imaging-confirmed NSCLC relapse, imaging was performed as clinically indicated. Detected clonal (circles, light blue) and subclonal (triangles, colors indicates different subclones) SNVs from each patient-specific assay-panel are plotted on graphs colored by M-Seq derived tumor phylogenetic nodes. Mean clonal (blue) and mean subclonal (red) plasma VAF are indicated on graphs as connected lines. Pre-operative and relapse M-Seq derived phylogenetic trees represented by ctDNA are illustrated above each graph.

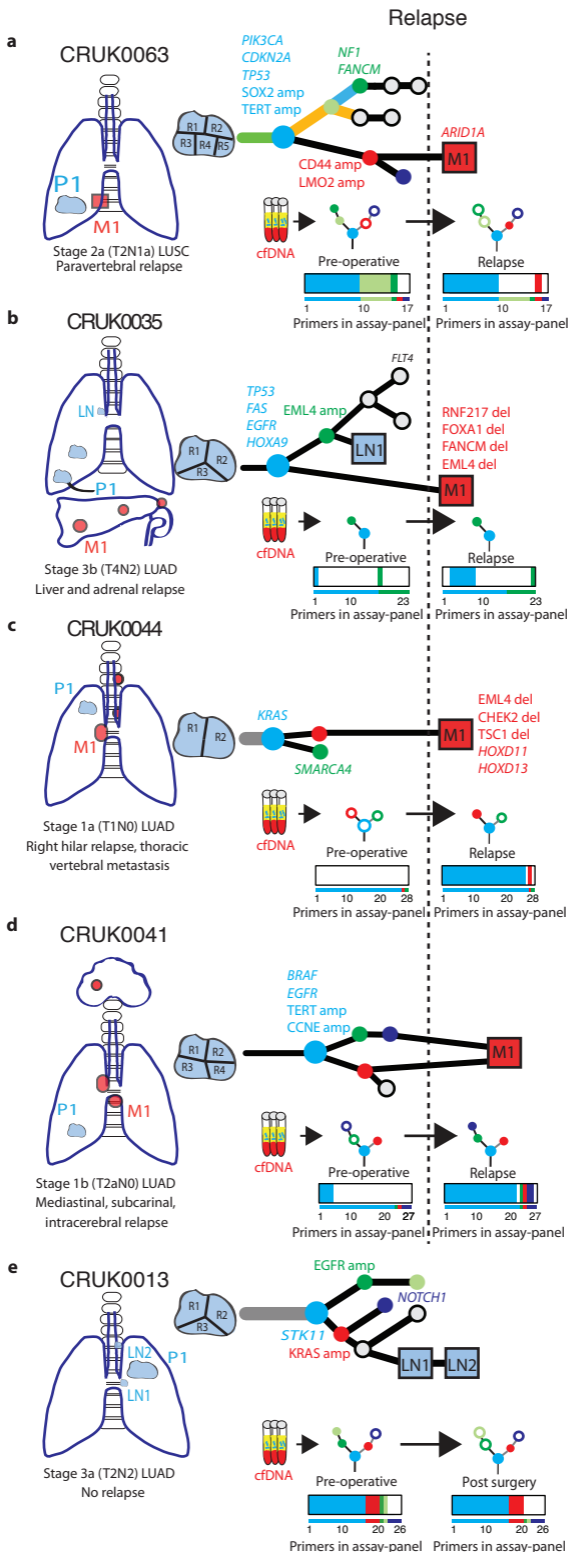


**Figure 5. Re-design of phylogenetic trees to incorporate relapse tissue sequencing data to benchmark post-operative ctDNA analyses**

Phylogenetic trees based on mutations found in primary and metastatic tissue (a-d), or primary tumor and lymph node biopsies (e). Colored nodes in phylogenetic trees indicate cancer clones harboring mutations assayed for in ctDNA, grey indicates a clone not assayed. Thick colored bar shows number of assays per sample detected preoperatively and at relapse (a-d) or in the absence of relapse, post surgery (e). Thin colored bar shows number of assays in total. Colors matches clones on the phylogenetic trees.

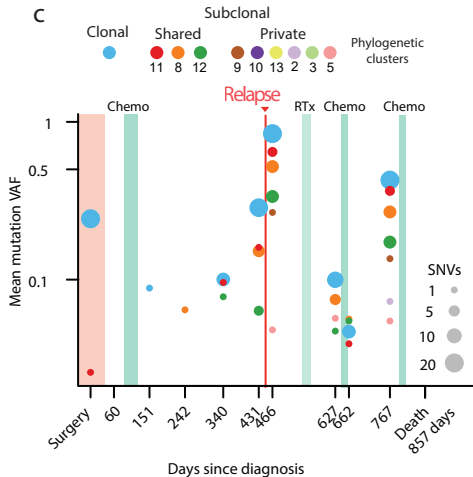
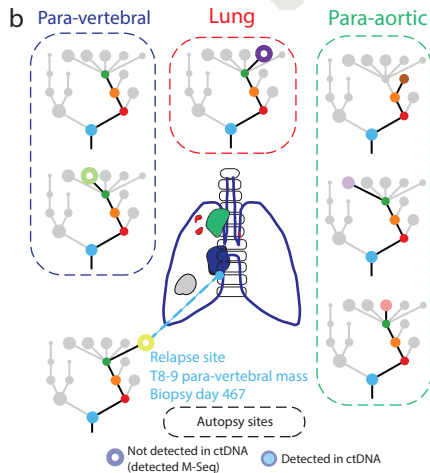
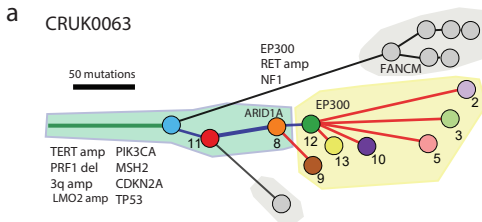


### **Figure 6. ctDNA tracking of lethal cancer subclones in CRUK0063**

Sampling and sequencing was performed of one relapse biopsy at day 467 and five metastatic tissue samples from three lesions at time of death through the PEACE (Posthumous Evaluation of Advanced Cancer Environment) post mortem study. Phylogenetic analysis revealed cancer evolution and identified private subclones at each site. **a)** To-scale phylogenetic tree of CRUK0063 including M-seq based on metastatic and primary tumor regions. Branch length is proportional to number of mutations in each subclone. Colors represents mutation clusters, light blue node representing the clonal cluster. **b)** Tissue-specific phylogenetic trees for metastatic lesions, highlighted nodes in color represents mutation clusters found at each site and assayed for in ctDNA. Open circles represents mutation clusters not detected at any time in ctDNA. **c)** Tracking plot of identified subclones in ctDNA, showing mean VAF of identified subclones. Size of dots indicates number of assays detected. Colors corresponds to mutation clusters and matches panels a and b. Tiered burden of subclonal disease can be observed, with clusters representing earlier cancer subclones present at higher VAF, likely reflecting a larger cancer burden carrying shared relative to private mutations.